マイクロピラー圧縮試験による鉄鋼材料の局所力学特性評価法の確立
Micro-scale Mechanical Response of Ferrous Materials Measured by Micropillar Compression Test

Naoki Takata
Associate professor, Dept. Materials and Sciences, Nagoya University

1. Introduction

Much previous research has been performed to assess the mechanical response of a variety of crystalline metals and alloys using micrometer and submicrometer-size pillars milled using a focurs ion beam (FIB) [1]. An attractive aspect of the micropillar compression test [2] is that this approach provides an opportunity to obtain fundamental single-crystal mechanical properties that are much difficult to determine for individual phases in multiphase materials. The extensive effort has been made to identify the scaling law for the strength of micrometer and submicrometer-sized specimens [1-13]. In aspects of the constitute phases in steels, microscale deformation behavior of ferrite (α-Fe) phase has been examined [1] as well as different bcc metals and alloys [1,14]. However, it is unclear whether the scaling law can valid for solid solution fcc phases corresponding to an austenite (γ-Fe) phase, since most of previous results have identified the scaling low for pure fcc metals (Au, Ni, Cu, Al) [2-13].

In process to prepare cylindrical micropillars on the sample surface, the incident FIB milling makes it inevitable to form micropillars with a trapezoidal cylinder shape [1], whereas the effect of shape parameters of micropillars on the measured strength has not been revealed. Such data are invaluable to understand the tolerance level of their shape parameters for measuring the reliable mechanical data of cylindrical micropillars.

In this study, the compression response of the γ-Fe (solid solution fcc) single-crystal micropillars with various sizes and shape parameters was examined using a γ-Fe single-phase steel, in comparison with the mechanical properties of millimeter-size specimens previously measured. These results were then utilized in conjunction with previous results on the scaling low for metals to understand the strength level of γ-Fe single-crystal cylindrical micropillars associated with their diameter and shape for determining the appropriate dimension of micropillars to measure the reliable mechanical data.

2. Experimental procedure

The nominal compositions (at.%) of the studied alloy was Fe–20Cr–30Ni. The alloy ingot was prepared by vacuum induction melting and were hot-forged at 1553 K into rods with a diameter of 12 mm. They were annealed at 1173K for 1 h. The observed sample surfaces were mechanically polished followed by electro-polishing in a solution of phosphoric acid with supersaturated Cr at 353 K, 1.8 A/cm^2 for 4 s. Their microstructures and fracture surfaces were observed by optical microscope and scanning electron microscopy (SEM: JEOL JSM-7000F) operated at 15 kV.

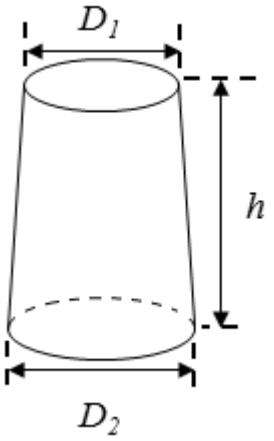

Fig.1 Schematics of the dimensional parameters of cylindrical micropillars prepared by focused ion beam in the present study.

Cylindrical micropillars with various diameters (approximately 1~10 μm) and shape parameters were fabricated on the sample surface by FIB milling (JEOL JIB-4601F) operated at 30 kV. The dimensional parameters of micropillars studied were schematically shown in Fig. 1. The top and bottom diameters of prepared micropillars with a trapezoidal cylinder shape were designated as D_1 and D_2, respectively. The specimen diameter (D) was used as the average value of D_1 and D_2 in present study. D_1, D_2 and height of micropillars (h) were measured using SEM images. These micropillars were compressed using a SHIMAZU DUH-211 dynamic ultra-micro tester equipped with a flat punch with a diameter of 20 μm in the load-control mode resulting in an initial strain rate of ~10^{-3} /s. In order to identify the compression direction, the crystallographic orientation of the γ-Fe phase was analyzed by electron-backscatter diffraction (EBSD) using the OIM Data Collection and OIM Data Analysis (TSL Solutions) software. The deformed micropillars were subsequently observed by SEM.

3. Results

3. 1 Single-crystal micropillars with different sizes

Fig. 2 illustrates γ-Fe single-crystal micropillars fabricated on the annealed sample of the Fe–20Cr–30Ni alloy. The observed SEM image (Fig. 2(a)) and corresponding orientation color map (Fig. 2(b)) obtained from EBSD analysis determine the crystallographic normal direction of the γ-Fe grains corresponding the compression direction of γ-Fe single-crystal micropillars fabricated on the sample surface. The following FIB milling on the particular grain can provide a number of cylindrical single-crystal micropillars with an identified compression direction (Fig. 2 (c,d)).

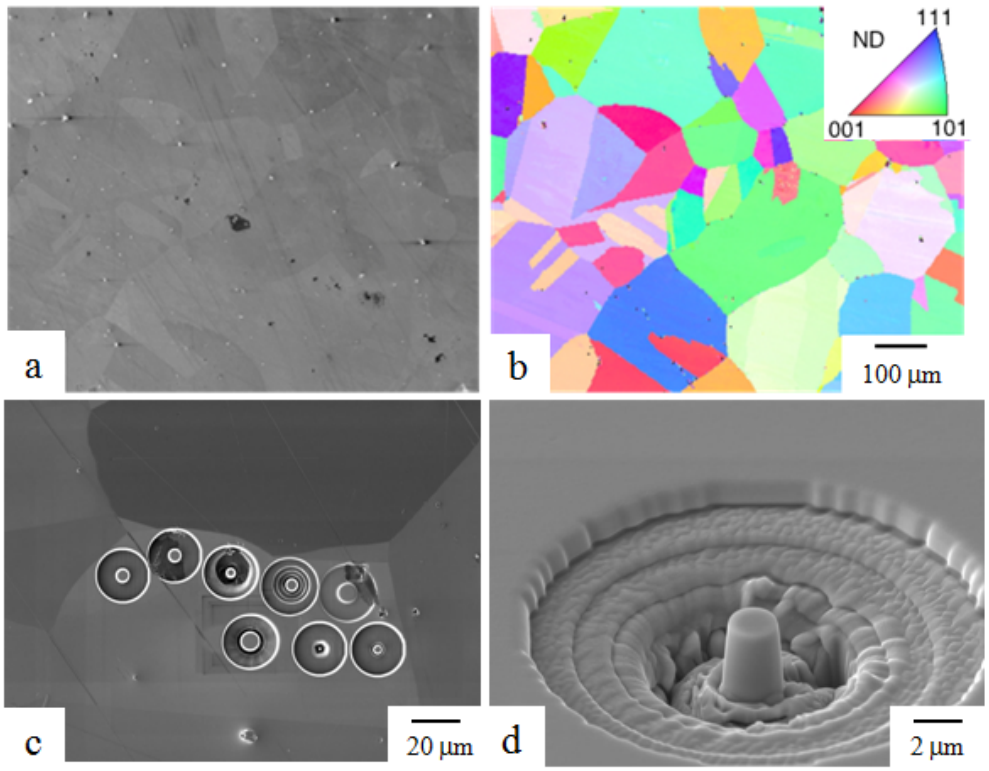

Fig. 2 (a) secondary electron image (SEI) showing microstructure and (b) corresponding orientation color map of the sample annealed at 1173 K for 1 h, (c, d) representative SEIs showing γ-Fe single crystal micropillars prepared on the sample.

Fig. 3 shows the representative nominal stress–strain curves of γ-Fe single-crystal micropillars with different diameters (D) ranging from 1.3 μm to 10.4 μm at room temperature. The compression direction indicated in an unit triangle of the inverse pole figure is close to [123] direction. There are distinct changes in the stress–strain curves of micropillars with smaller size. The micropillar with D = 1.3 μm exhibits an incrementally rising flow curve with rapid strain bursts that proceeds to a magnitude of a few percent at several stress levels. A similar flow response was observed for micropillars with smaller sizes than 2 μm.

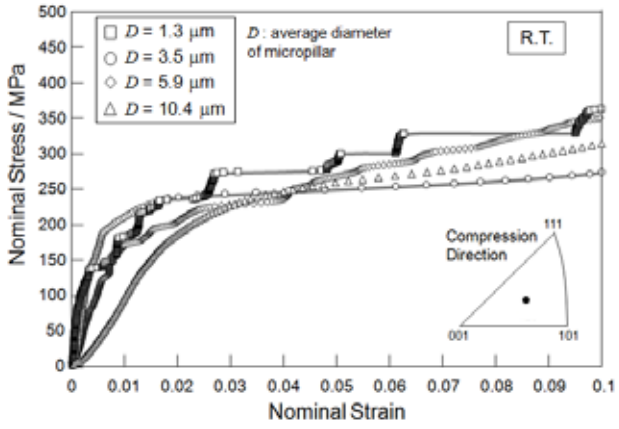

Fig. 3 Nominal stress-strain curves of γ-Fe single crystal micropillars with various diameters (D) at room temperature. The compression direction is close to [123] direction.

However, there are the more scarcely rapid strain bursts for the larger-sized micropillars. The flow curve of the micropillar with D = 3.5 μm exhibits a continuous yielding of approximately 190 MPa, followed by a large strain excursion at 230 MPa that would corresponds to the typical single-slip. The following slight strain-hardening was observed at higher strain regime. The continuous flow curves were observed for the larger-size micropillars. There was not a detectable systematic variation in the flow stress level depending on the mean diameter of micropillars, although the higher strength of smaller-size specimen is generally understood [1]. Note that the lower slope of the elastic portion was found in larger-size micropillars, which might be attributed to the compliance associated with the stiffness of γ-Fe phase underneath the micropillars compressed [3].

Fig. 4 presents secondary electron images (SEIs) showing the single-crystal micropillars before and after the compression test. Obvious differences were observed in the appearance of the micropillar with D = 1.3 μm after testing. The compressed micropillar exhibits a couple of distinct shear surfaces (Fig. 4(b)), indicating large single-slip-plane displacements under compression loading, which is represented by rapid strain bursts in the flow curve (Fig. 3). Fine discrete slip bands were observed along the gauge portion of the cylindrical micropillar with D = 3.5 μm (Fig. 4(d)), whereas the localization of the slip surface was scarcely observed. In micropillars with larger D (Fig. 4 (f,h)), slip traces on a single plane was observed on the whole surface of the micropillars. Note that secondary-slip traces were locally observed on the surface of all micropillars, which is indicative of the strain-hardening at high strain regime (Fig. 3).

Fig. 5 presents SEIs showing a representative micropillar compressed, together with 111 and 110 pole figures indicating the activate slip plane and direction, respectively. The measured angle between compression axis and slip trace lines (Fig. 5(a)) is close to one between compression axis and a (111) plane determined by the 111 pole figure (Fig. 5(c)) obtained from the prior EBSD analysis. The top view of the compressed micropillar represents the shear direction due to a primary single-slip (Fig. 5(b)). The direction corresponds well to a [-101] direction indicating on the stereographic projection (Fig. 5(d)). These comparisons determine an activated primary slip system of (111)[-101] in the single-crystal micropillars under the compression loading, which is a most favorable slip system for the activation in terms of Schmid factor.

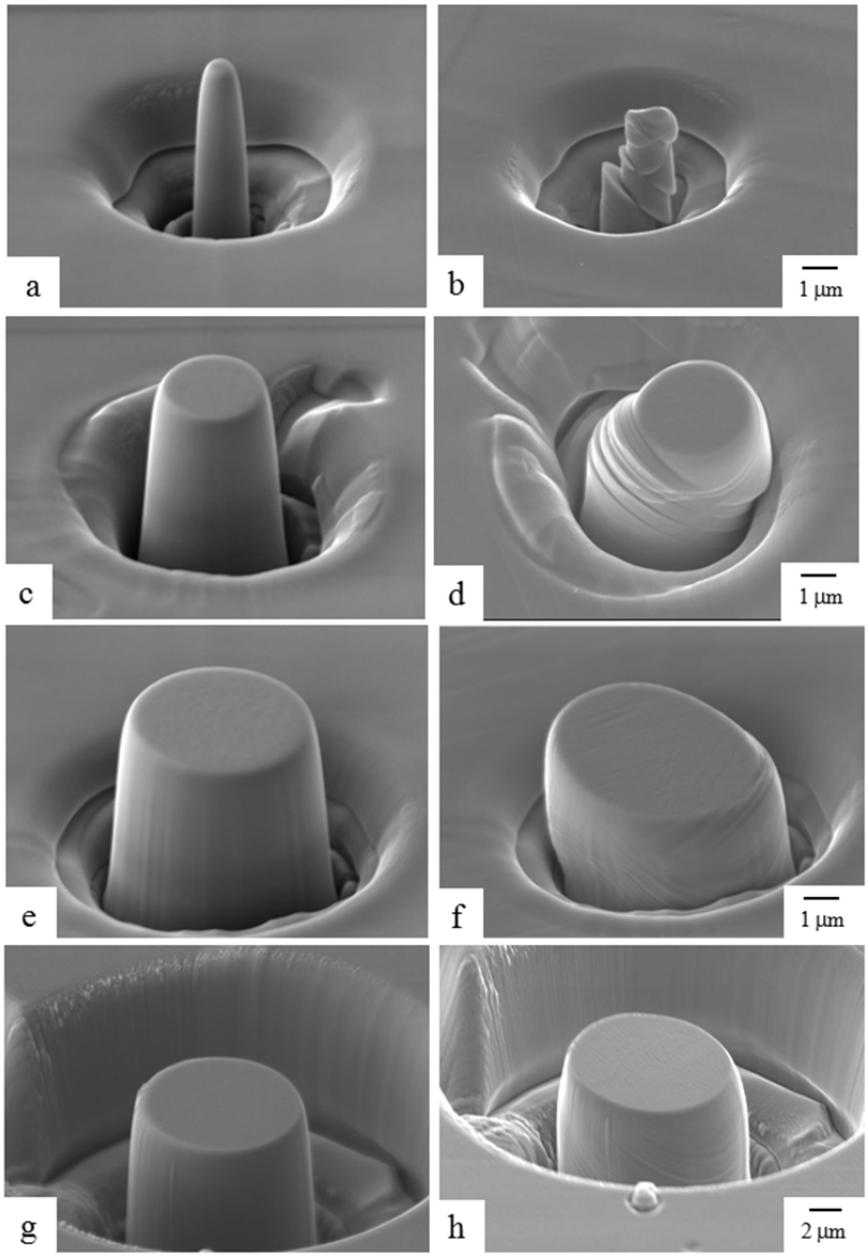

Fig. 4 SEIs showing the γ-Fe single crystal cylindrical micropillars with various diameters (D) before (a, c, e, g) and (b, d, f, h) after the compression test: (a, b) D = 1.2 μm, (c, d) D = 3.5 μm, (e, f) D = 5.9 μm, (g, h) D = 10.4 μm.

Fig. 6 shows changes of the 0.2 % proof stress ($\sigma_{0.2\%}$) and the stress at a strain of 5% ($\sigma_{5\%}$) determined from the stress–strain curves (as shown in Fig. 3) as a function of mean diameter (D) of cylindrical micropillars. The clear size dependences of $\sigma_{0.2\%}$ and $\sigma_{5\%}$ were not found in the mean diameters approximately ranging from 1 μm to 10 μm. $\sigma_{0.2\%}$ and $\sigma_{5\%}$ were nearly constant of around 160 MPa and 270 MPa respectively, independent of D, whereas a trend of relatively scattered $\sigma_{0.2\%}$ values at smaller D than 2 μm was also found.

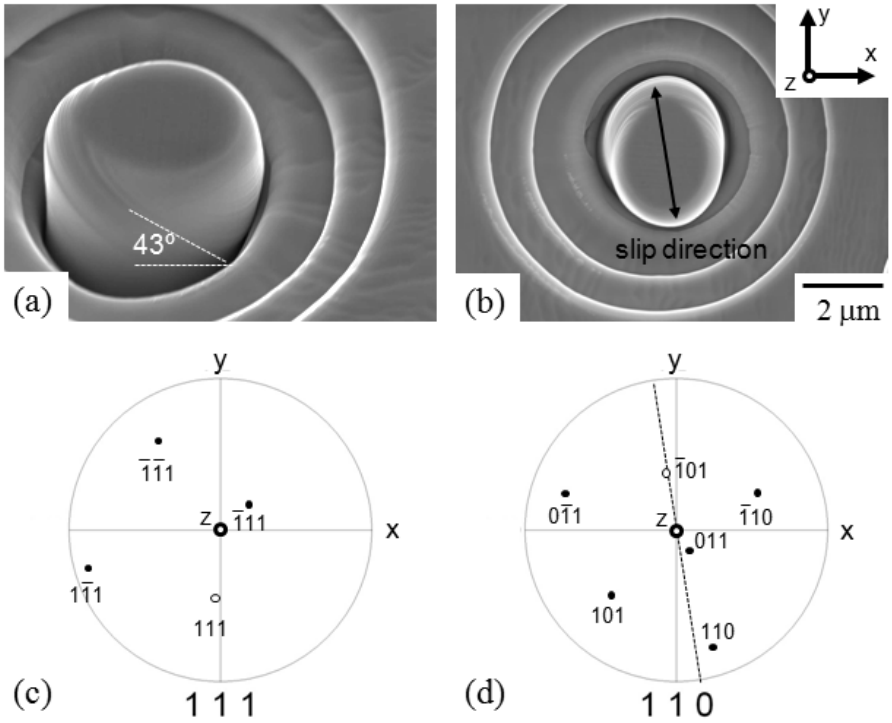

Fig. 5 (a, b) SEI showing the compressed micropillar and (c, d) corresponding 111 and 011 poles indicated on the stereographic projection. (The angles between observation and the compression directions in (a) and (b) are 53degrees and 0 degrees, respectively.)

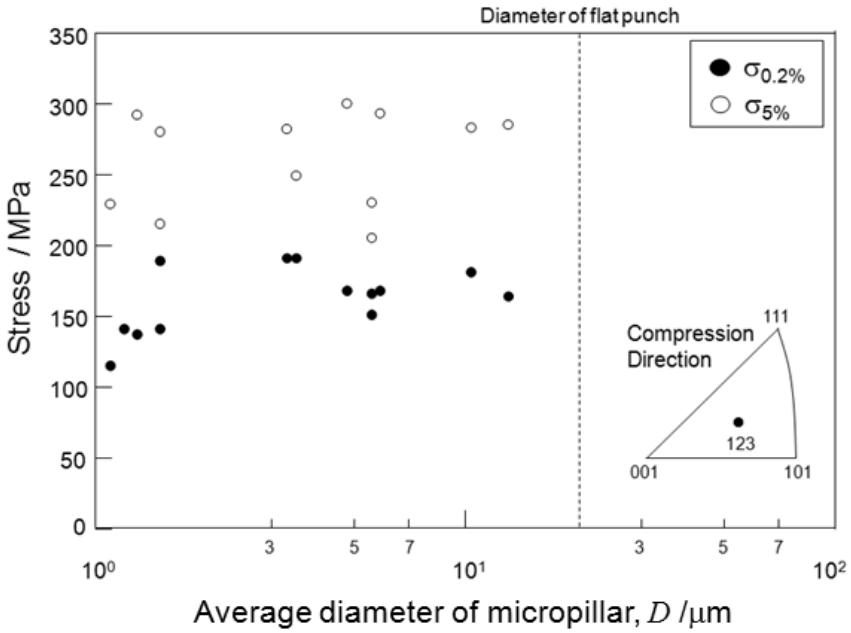

Fig. 6 Change in 0.2% and 0.5 % proof stresses as a function of average diameter of the cylindrical γ-Fe single crystal micropillar (D).

3. 2 Single-crystal micropillars with different shapes

Fig. 7 shows the representative nominal stress–strain curves of γ-Fe single-crystal micropillars with different trapezoidal-cylinder shape parameters designated as D_1/D_2 at room temperature. The compression direction is close to [123] direction as well. In this figure, the mean diameter (D) was used to prepare the stress–strain curves from the load–displacement curves measured in the present study. Note that the mean diameters of these micropillars were around 3 μm (ranges from 2.9 to 3.5 μm). The micropillar with $D_1/D_2 = 0.75$ exhibits a continuous yielding of approximately 190 MPa, followed by a large displacement due to the activation of single-slip system. In the micropillar with D_1/D_2 = 0.54, the flow curve shows a rapid strain burst at a lower stress of about 120 MPa. The strain bursts were found at higher strain regime as well. In the micropillar with smaller D_1/D_2, the strain burst occurs at much lower stress followed by the increase in the stress under loading.

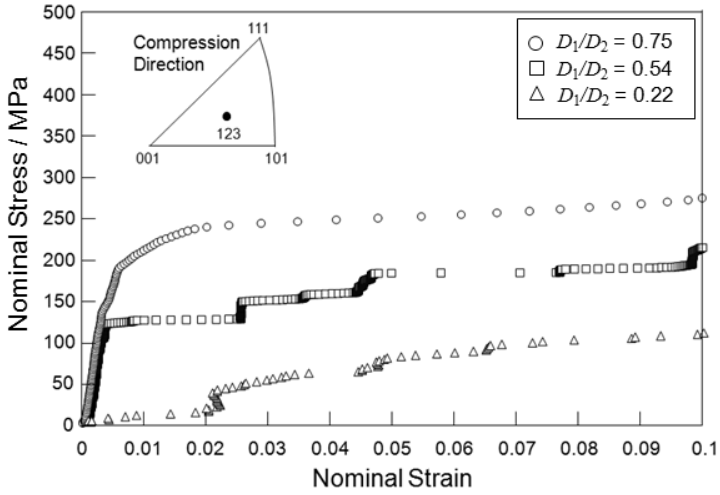

Fig. 7 Nominal stress-strain curves of γ-Fe single crystal micropillars with different dimensional parameters at room temperature (average diameter of these micropillars are approximately 3 μm).

Fig. 8 presents SEIs showing the micropillars with different values of D_1/D_2 before and after the compression test. The clear slip traces on a single plane corresponding to the activation of the primary slip were observed on the whole surface of the micropillar with $D_1/D_2 = 0.54$, whereas local slip traces on the different plane corresponding to the secondary slip system appears around the top surface of the micropillar (Fig. 8(b)). The obvious shear surface was localized around the tip (top portion) of a distinctive trapezoidal-cylinder-shaped micropillar with $D_1/D_2 = 0.22$ (Fig. 8(d)). The shear surface morphology is similar to that observed on the surface of micropillars with smaller diameter than 2 μm (Fig. 4(b)). The slip traces appears only on the specimen surface of top portion as well.

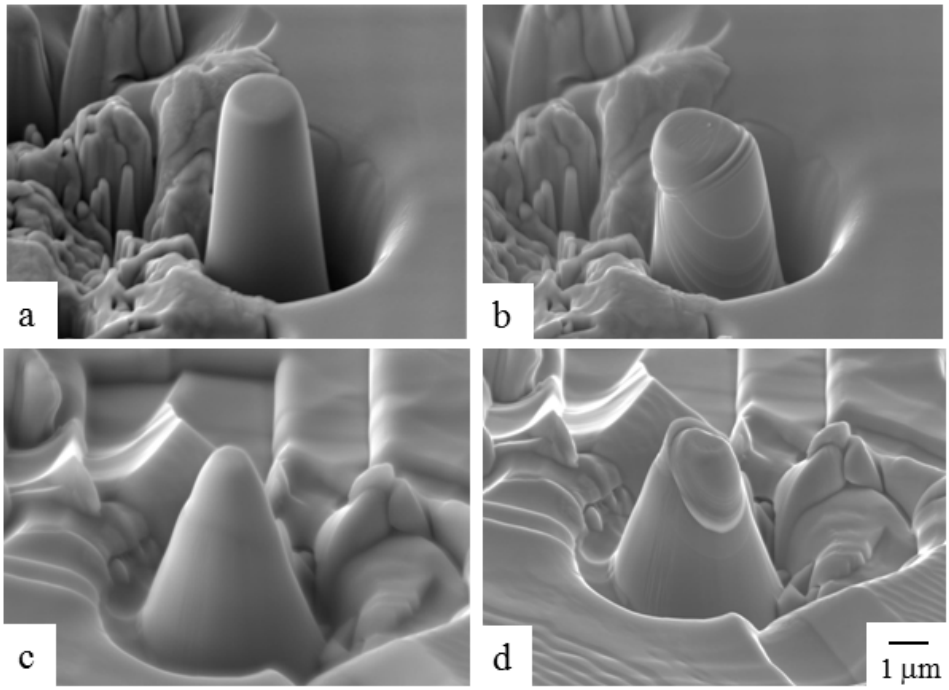

Fig. 8 SEIs showing the γ-Fe single crystal micropillars with various dimensional parameter (D_1/D_2) before (a, c) and (b, d) after the compression test: (a, b) D_1 = 2.2 μm and D_2 = 3.7 μm, (c, d) D_1 = 0.9 μm and D_2 = 4.1 μm.

Fig. 9 shows a variation in the 0.2 % proof stress ($\sigma_{0.2\%}$) of micropillars with mean diameters ranging from 2.5 to 5.9 μm as a function of D_1/D_2. The value of $\sigma_{0.2\%}$ is almost constant of approximately 170 MPa at higher D_1/D_2 than 0.6, whereas it becomes significantly lower at lower D_1/D_2 than 0.6. This result clearly indicates the critical D_1/D_2 value for measuring the accurate stress level of cylindrical micropillars with several micrometer-sizes.

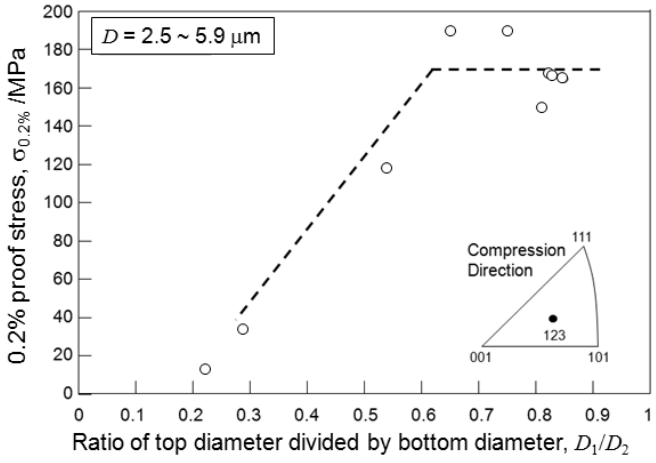

Fig. 9 Change in 0.2 % proof stress (yield stress) as a function of the ratio of top diameter divided by bottom diameter of micropillars (D_1/D_2).

4. Discussion

The present study investigated the strength level of γ-Fe single-crystal cylindrical micropillars depending on their diameter and shape in comparison with the millimeter-size polycrystalline specimens. One of interesting findings in this study is a nearly constant strength level of γ-Fe single-crystal micropillars independent of their mean diameter (specimen size) approximately ranging from 1 μm to 10 μm (Fig. 6), which is different from a general trend on the size dependence for the strength of fcc metals [1,10]. However, the compressed micropillars with a smaller diameter than 2 μm appears the significant shear-surfaces on a (111) plane (Fig. 4 (b)) corresponding to the occurrence of rapid strain-bursts, which is a typical deformation behavior of the submicron or nanometer-size specimens [1,2]. The measured strength level of the γ-Fe single-crystal micropillars is discussed in terms of the scaling low for fcc metals previously proposed [1, 10] as follows.

Previous systematic studies have summarized the compressive strength for single-crystal pure fcc metals (Au, Al, Ni, and Cu) with sub-micron size and proposed a universal scaling law for the strength of fcc metals [10] as follows:

$$\tau_{res} / \mu = A (D/b)^m \quad (1)$$

where μ is the shear modulus, τ_{res} is the resolved shear stress on {111} slip planes to <110> directions, D is the pillar diameter, and b is the magnitude of the Burgers vector. On the basis of the experimental data, the A and m were measured to be 0.71 and -0.66, respectively. It was found that the scaling law is satisfied at lower D/b than approximately 3×10^4 [10], corresponding to the pillar diameter smaller than approximately 8 μm. In order to compare the scaling law for the strength with the measured strength level of γ-Fe single-crystal micropillars, the resolved shear stresses of micropillars calculated using their $\sigma_{0.2\%}$ (Fig. 6) and Schmid factor (Fig. 5) were plotted as a function of the mean micropillar diameter (D), together with the estimated shear strength level of millimeter-size specimens. This result is shown in Fig. 10. In this figure, the σ_0 value of 122 MPa in the 0.2% proof stress previously measured is indicated as well. In the mean diameter smaller than 3 μm, the experimentally measured resolved shear stress is much lower than the strength level calculated based on the proposed scaling law (equation (1)), whereas the measured shear stress is located on the trend line following the scaling law in a pillar diameter range from 3 μm to 6 μm. In case of larger diameter than 10 μm, it might be difficult to compare the measured data with the scaling law, because of the size limitation (smaller than approximately 8 μm) for satisfying the scaling law [10]. Note that the measured resolved shear stress is approximately twice higher than the estimated shear stress of

millimeter-size specimens. These results indicate that the strength would be significantly reduced in the γ-Fe single-crystal micropillars with smaller sizes below 3 μm, which is deviated from the scaling law for the strength of fcc metals reported in the literature [1,10]. One of possible contributors to reduce the strength is FIB damage accumulated in the surface layer of γ-Fe micropillars fabricated [15, 16], whereas the detailed mechanism is still in question. The minute observation of lattice defects in TEM thin film samples prepared by different processes of FIB milling and electro-polishing would be required to identify whether any damage are introduced into the fcc solid solution of γ-Fe phase by FIB milling. This would await the future work to understand the unique scaling law for the strength of γ-Fe phase.

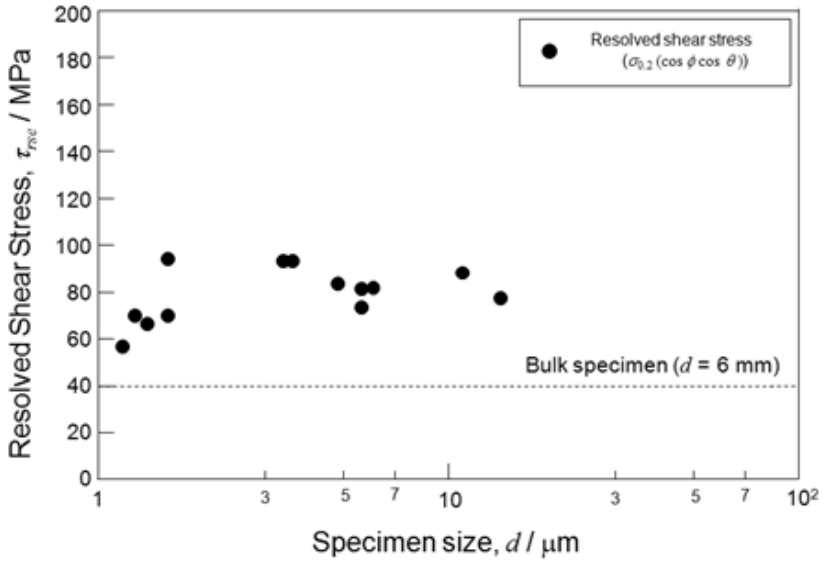

Fig. 10 Change in resolved shear stress of γ-Fe single crystal micropillars as a function of average specimen diameter.

Acknowledgments

The support of JFE 21st Century Foundation is gratefully acknowledged.

References

1) Julia R. Greer, Jeff Th.M. De Hosson, Plasticity in small-sized metallic systems: Intrinsic versus extrinsic size effect, Prog. Mater. Sci., 56 (2011), 654-724.
2) Michael D. Uchic, Dennis M. Dimiduk, Jeffrey N. Florando, William D. Nix, Sample Dimensions Influence Strength and Crystal Plasticity, Science, 305 (2004), 986-989.
3) Julia R. Greer, Warren C. Oliver, William D. Nix, Size dependence of mechanical

properties of gold at the micron scale in the absence of strain gradients, Acta Mater., **53** (2005) 1821–1830.

4) D.M. Dimiduk, M.D. Uchic, T.A. Parthasarathy, Size-affected single-slip behavior of pure nickel microcrystals, Acta Mater. **53** (2005) 4065–4077.
5) Julia R. Greer, William D. Nix, Nanoscale gold pillars strengthened through dislocation starvation, PHYSICAL REVIEW B **73** (2006) 245410.
6) Triplicane A. Parthasarathy, Satish I. Rao, Dennis M. Dimiduk, Michael D. Uchic and Dallas R. Trinkle, Contribution to size effect of yield strength from the stochastics of dislocation source lengths in finite samples, Scripta Mater. **56** (2007) 313–316.
7) S.I. Rao, D.M. Dimiduk, T.A. Parthasarathy, M.D. Uchic, M. Tang, C. Woodward, Athermal mechanisms of size-dependent crystal flow gleaned from three-dimensional discrete dislocation simulations, Acta Mater. **56** (2008) 3245–3259.
8) D.M. Norfleet, D.M. Dimiduk, S.J. Polasik, M.D. Uchic, M.J. Mills, Dislocation structures and their relationship to strength in deformed nickel microcrystals, Acta Mater. **56** (2008) 2988–3001.
9) C.P. Frick, B.G. Clark, S. Orso, A.S. Schneider, E. Arzt, Size effect on strength and strain hardening of small-scale [1 1 1] nickel compression pillars, Mater. Sci. Eng. A **489** (2008) 319–329.
10) R. Dou, B. Derby, A universal scaling law for the strength of metal micropillars and nanowires, Scripta Mater. **61** (2009) 524–527.
11) Andrew T. Jennings, Michael J. Burek, Julia R. Greer, Microstructure versus Size: Mechanical Properties of Electroplated Single Crystalline Cu Nanopillars, PHYSICAL REVIEW LETTERS, **104** (2010), 135503.
12) William D. Nix, Seok-Woo Lee, Micro-pillar plasticity controlled by dislocation nucleation at surfaces, Phil. Mag. **91** (2011), 1084–1096.
13) Qiaoyan Sun, Qiang Guo, Xi Yao, Lin Xiao, Julia R. Greer, Jun Sun, Size effects in strength and plasticity of single-crystalline titanium micropillars with prismatic slip orientation, Scripta Mater. **65** (2011), 473-476.
14) A.S. Schneider, C.P. Frick, B.G. Clark, P.A. Gruber, E. Arzt, Influence of orientation on the size effect in bcc pillars with different critical temperatures, Mater. Sci. Eng. A **528** (2011), 1540-1570.
15) S. Shim, H. Bei, M.K. Miller, G.M. Pharr, E.P. George, Effects of focused ion beam milling on the compressive behavior of directionally solidified micropillars and the nanoindentation response of an electropolished surface, Acta Mater. **57** (2009)

503–510.

16) J. Zimmermann, S. Van Petegem, H. Bei, D. Grolimund, E.P. George, H. Van Swygenhoven, Effects of focused ion beam milling and pre-straining on the microstructure of directionally solidified molybdenum pillars: A Laue diffraction analysis, Scripta Mater. **62** (2010) 746–749.